5022 *Chem. Mater.* **2009,** *21,* 5022–5031
DOI:10.1021/cm9013514

CHEMISTRY OF MATERIALS
Article

Electrodeposition of Epitaxial Magnetite Films and Ferrihydrite Nanoribbons on Single-Crystal Gold

Elizabeth A. Kulp, Hiten M. Kothari, Steven J. Limmer, Jinbo Yang, Rakesh V. Gudavarthy, Eric W. Bohannan, and Jay A. Switzer*

Department of Chemistry, Missouri University of Science and Technology, 103 Materials Research Center, Rolla, Missouri 65409-1170

Received May 15, 2009. Revised Manuscript Received September 18, 2009

Magnetite (Fe_3O_4), ferrihydrite ($Fe_{10}O_{14}(OH)_2$), and iron (Fe) films were electrodeposited by cathodic deposition from an alkaline Fe(III)−triethanolamine solution. The electrodeposited phase depended on the applied potential. Magnetite films were electrodeposited from −1.01 to −1.10 V vs Ag/AgCl, whereas ferrihydrite films were deposited from −1.10 to −1.20 V vs Ag/AgCl. Iron deposition occurred at more negative potentials. The polycrystalline films were characterized using X-ray diffraction, scanning electron microscopy, and Mössbauer spectroscopy. Epitaxial magnetite films on low-index gold crystals were produced at three different potentials. X-ray diffraction analysis of the magnetite films deposited at −1.01, −1.05, and −1.10 V vs Ag/AgCl showed [111] oriented films on Au(111) and Au(001). Because of twinning of the {111} planes, the [511] orientation was present in thicker films. Magnetite grew with a [110] orientation on Au(110). At the more negative potentials of −1.10 and −1.20 V vs Ag/AgCl, ferrihydrite deposited with an $(11\bar{2}0)$ orientation.

Introduction

Abundant in nature, iron oxides, including iron hydroxides and iron (oxy)hydroxides, have been used as catalysts, pigments, and magnetic coatings due to their chemical and physical properties.[1,2] The iron oxide magnetite (Fe_3O_4) is a ferrimagnetic material with an inverse spinel structure, space group $Fd\bar{3}m$. This mixed-valence transition metal oxide has Fe^{3+} and Fe^{2+} ions in the octahedral sites and Fe^{3+} ions in the tetrahedral sites. For Fe_3O_4, ferrimagnetism is observed below the Curie temperature of 860 K.[1] Calculations have also indicated that the Fermi level electrons are 100% spin-polarized in this ferrimagnetic phase.[3,4] In the ideal case of stoichiometric magnetite, the moments of the Fe^{3+} ions are antiferromagnetically coupled and the resulting magnetic moment is due to the Fe^{2+} in the cell. The electrical conductivity of this material at room temperature is reportedly the result of hopping of the charge carriers between the Fe^{2+} and Fe^{3+} ions in the octahedral sites.[4,5] As the temperature drops below 120 K, a metal to insulator transition known as the Verwey transition occurs.[6] This charge-ordered insulator has a magnetoelectronic effect, becoming ferroelectric below this Verwey temperature.[7−9] These properties make magnetite a potential candidate for applications in magnetic memory, magnetoreceptors, and spin-dependent transport devices.[10−24]

*To whom correspondence should be addressed. E-mail: jswitzer@mst.edu.

(1) Cornell, R. M.; Schwertmann, U. *The Iron Oxides: Structure, Properties, Reactions, Occurrences, and Uses*; VCH: Weinheim, Germany, 1996.
(2) Schwertmann, U.; Cornell, R. M. *Iron Oxides in the Laboratory: Prepartion and Characterization*, 2nd ed.; Wiley: New York, 2000.
(3) Zhang, Z.; Satpathy, S. *Phys. Rev. B* **1991**, *44*, 13319.
(4) Anisimov, V. I.; Elfimov, I. S.; Hamada, N.; Terakura, K. *Phys. Rev. B* **1996**, *54*, 4387.
(5) Yanase, A.; Siratori, K. *J. Phys. Soc. Japan* **1984**, *53*, 312.
(6) Verwey, E. J. W. *Nature* **1939**, *144*, 327.
(7) Walz, F. J. *Phys.: Condens. Matter*. **2002**, *14*, R285.
(8) Garcia, J.; Subias, G. J. *Phys.: Condens. Matter*. **2004**, *16*, R145.
(9) Rado, G. T.; Ferrari, J. M. *Phys. Rev. B* **1977**, *15*, 290.
(10) Miyamoto, Y.; Ishihara, S.; Hirano, T.; Takada, M.; Suzuki, N. *Solid State Commun*. **1994**, *89*, 51.
(11) Lee, S.; Fursina, A.; Mayo, J. T.; Yavuz, C. T.; Colvin, V. L.; Sofin, R. G. S.; Shvets, I. V.; Natelson, D. *Nat. Mater*. **2008**, *7*, 130.
(12) van den Brink, J.; Khomskii, D. I. J. *Phys.: Condens. Matter* **2008**, *20*, 434217/1.
(13) Prinz, G. A. *Science* **1998**, *282*, 1660.
(14) Wolf, S. A.; Awschalom, D. D.; Buhrman, R. A.; Daughton, J. M.; von Molnar, S.; Roukes, M. L.; Chtchelkanova, A. Y.; Treger, D. M. *Science* **2001**, *294*, 1488.
(15) Kirshvink, J. L., Jones, D. S., MacFadden, B. J. Eds. *Magnetite Biomineralization and Magnetoreception in Organisms: A New Biomagnetism*; Plenum: New York, 1985.
(16) Wiltschko, R.; Wiltschko, W. *Magnetic Orientation in Animals*; Springer: New York, 1995.
(17) Mora, C. V.; Davison, M.; Wild, J. M.; Walker, M. M. *Nature* **2004**, *432*, 508.
(18) Walker, M. M.; Kirschvink, J. L.; Chang, S.-B. R.; Dizon, A. E. *Science* **1984**, *224*, 751.
(19) Scheffel, A.; Gruska, M.; Faivre, D.; Linaroudis, A.; Plitzko, J. M.; Schüler, D. *Nature* **2006**, *440*, 110.
(20) Johnsen, S.; Lohmann, K. J. *Phys. Today* **2008**, *31*, 29.
(21) Fleissner, G.; Stahl, B.; Thalau, P.; Falkenberg, G.; Fleissner, G. *Naturwissenschaften* **2007**, *94*, 631.
(22) Xu, Y. B.; Ahmad, E.; Claydon, J. S.; Lu, Y. X.; Hassan, S. S. A.; Will, I. G.; Cantor, B. *J. Magn. Magn. Mater*. **2006**, *304*, 69.
(23) Cheong, S.-W.; Mostovoy, M. *Nat. Mater*. **2007**, *6*, 13.
(24) Béa, H.; Gajek, M.; Bibes, M.; Barthélémy, A. *J. Phys.: Condens. Matter* **2008**, *20*, 434221/1.

 Published on Web 10/07/2009

One method to produce magnetite is electrodeposition.[25−35] Magnetite has been deposited by electrochemically oxidizing Fe(II)[25−33] or reducing Fe(III)[34,35] at the electrode surface, followed by a chemical reaction between the generated species and the original cation to produce a film. Previous work by this research group has shown that epitaxial films of Fe_3O_4 on gold single crystals can be produced by anodic deposition from a Fe(II) deposition bath.[26] However, the Fe(II) deposition bath is unstable at high temperatures, reacting with the oxygen in air to produce Fe_3O_4 powder. Sapieskzko and Matijevic developed a hydrothermal method to produce Fe_3O_4 powder from Fe(III)−triethanolamine solutions using reducing agents and thermal decomposition.[36] We have modified this solution and shown that Fe_3O_4 films can be electrodeposited onto polycrystalline stainless steel electrodes at a constant cathodic current density of 2 mA/cm^2.[34]

Another iron compound, ferrihydrite, is a poorly crystalline material with various reported chemical formulas such as $Fe_5HO_8\cdot 4H_2O$, $5Fe_2O_3\cdot 9H_2O$, and $Fe_2O_3\cdot 2FeOOH\cdot 2.6H_2O$.[1,37] Recently, a proposed chemical formula and structure of $Fe_{10}O_{14}(OH)_2$ (space group, $P6_3mc$) was developed using synchrotron data;[38,39] however, this study has already been questioned.[40] Owing to its poor crystalline quality, ferrihydrite is further labeled as 2-line or 6-line ferrihydrite based on the number of observed peaks in the X-ray diffraction pattern.[1,2,37] Ferrihydrite is superparamagnetic at room temperature and shows magnetic ordering at 4.2 K.[1,37,41] It is observed in the corrosion of iron and steel and as a byproduct in mining.[37] Also found in soil and sediments, this nanomaterial naturally adsorbs cations, anions, and organic species such as insecticides and herbidices.[37] Because of this adsorption, ferrihydrite has been studied for the removal of heavy metals in water treatment[37] and SO_2 emission.[42] This material is also suggested as the iron core of ferritin, an iron storage protein.[43] Generally, this metastable material is made synthetically by rapid oxidation of Fe(II) or by hydrolysis of Fe(III) salts.[1,2,37] It is then used as a precursor for the production of goethite and hematite.[1,2,37]

Although various methods are used to produce iron compounds, this paper offers a novel approach to produce both magnetite (Fe_3O_4) and ferrihydrite ($Fe_{10}O_{14}(OH)_2$) electrochemically from the same alkaline Fe(III)−triethanolamine deposition bath. In this bath, Fe(III) is electrochemically reduced to Fe(II). Therefore, the concentration of the Fe(II) at the electrode surface is controlled by the applied potential. The ability to change the Fe(II) surface concentration by changing the applied potential permits the electrodeposition of magnetite films with varying stoichiometries from −1.01 to −1.10 V vs Ag/AgCl, and the deposition of ferrihydrite films at potentials from −1.10 to −1.20 V vs Ag/AgCl. These films are characterized as a function of applied potential by X-ray diffraction (XRD), scanning electron microscopy (SEM), and Mössbauer spectroscopy. Films of these materials electrodeposited on low index gold crystals are epitaxial as characterized by XRD and SEM.

Experimental Section

The deposition bath was prepared by dissolving 2.6 g of iron(III) sulfate hydrate in 15 ml of 1 M triethanolamine (TEA), resulting in a deep red colored solution. This solution was diluted with 50 ml of distilled, deionized water. It was then added to a second solution of 12.0 g of NaOH pellets in 85 ml of distilled, deionized water. The resulting gray-green solution was heated to 80 °C. All chemicals were ACS reagent grade and purchased from Sigma-Aldrich. The water was produced in house by a Millipore system (18 MΩ-cm).

For characterization, films were deposited on 430 stainless steel substrates. The 430 stainless steel substrates were mechanically polished and sonicated in acetone and deionized water. The films were deposited on these substrates and rinsed with 80 °C distilled, deionized water. The defect chemistry of the magnetite films was controlled using constant potentials between −1.00 and −1.10 V vs Ag/AgCl. Ferrihydrite films were deposited from −1.10 to −1.20 V vs Ag/AgCl. For epitaxial studies, films were eletrodeposited on gold single crystals. The gold crystals were electropolished with a solution of 100 ml of ethanol, 50 ml of ethylene glycol, and 50 ml of concentrated hydrochloric acid and heated to 55 °C. Each gold crystal was positioned in this stirred solution to form a meniscus in the electropolishing solution. An anodic constant current density of 1.6 A/cm^2 was applied for 45 s. The single crystals were thoroughly rinsed with ethanol and water. The epitaxial films were deposited at −1.01, −1.05, −1.10, and −1.20 V vs Ag/AgCl and rinsed with 80 °C distilled, deionized water.

(25) Abe, M.; Tamaura, Y. *J. Appl. Phys.* **1983**, *22*, L511.
(26) Sorenson, T. A.; Morton, S. A.; Waddill, D. G.; Switzer, J. A. *J. Am. Chem. Soc.* **2002**, *124*, 7604.
(27) Carlier, D.; Terrier, C.; Arm, C.; Ansermet, J.-P. *Electrochem. Solid State Lett.* **2005**, *8*, C43.
(28) Nishimura, K.; Kitamoto, Y.; Abe, M. *IEEE Trans. Magn.* **1999**, *35*, 3043.
(29) Peulon, S.; Antony, H.; Legrand, L.; Chausse, A. *Electrochim. Acta* **2004**, *49*, 2891.
(30) Wang, S.-Y.; Ho, K.-C.; Kuo, S.-L.; Wu, N.-L. *J. Electrochem. Soc.* **2006**, *153*, A75.
(31) Martinez, L.; Leinen, D.; Martin, F.; Gabas, M.; Ramos-Barrado, J. R.; Quagliata, E.; Dalchiele, E. A. *J. Electrochem. Soc.* **2007**, *154*, D126.
(32) Chatman, S.; Noel, A. J. G.; Poduska, K. M. *J. Appl. Phys.* **2005**, *98*, 113902.
(33) Teng, C.-L.; Ryan, M. P. *Electrochem. Solid State Lett.* **2007**, *10*, D108.
(34) Kothari, H. M.; Kulp, E. A.; Limmer, S. J.; Poizot, P.; Bohannan, E. W.; Switzer, J. A. *J. Mater. Res.* **2006**, *21*, 293.
(35) Mitra, S.; Poizot, P.; Finke, A.; Tarascon, J.-M. *Adv. Funct. Mater.* **2006**, *16*, 2281.
(36) Sapieszko, R. S.; Matijevic, E. *J. Colloid Interface Sci.* **1980**, *74*, 405.
(37) Jambor, J. L.; Dutrizac, J. E. *Chem. Rev.* **1998**, *98*, 2549.
(38) Michel, F. M.; Ehm, L.; Antao, S. M.; Lee, P. L.; Chupas, P. J.; Liu, G.; Strongin, D. R.; Schoonen, M. A. A.; Phillips, B. L.; Parise, J. B. *Science*. **2007**, *316*, 1726.
(39) Michel, F. M.; Ehm, L.; Liu, G.; Han, W. Q.; Antao, S. M.; Chupas, P.J.; Lee, P. L.; Knorr, K.; Eulert, H.; Kim, J.; Grey, C. P.; Celestian, A. J.; Gillow, J.; Schoonen, M. A. A.; Strongin, D. R.; Parise, J. B. *Chem. Mater.* **2007**, *19*, 1489.
(40) Rancourt, D. G.; Meunier, J.-F. *Am. Mineral.* **2008**, *93*, 1412–1417.
(41) Pankhurst, Q. A.; Pollard, R. J. *Clays and Clay Minerals* **1992**, *40*, 268–272.
(42) G. Liu, G.; Debnath, S.; Paul, K. W.; Han, W.; Hausner, D. B.; Hosein, H.-A.; Michel, F. M.; Parise, J. B.; Sparks, D. L.; Strongin, D. R. *Langmuir* **2006**, *22*, 9313–9321.
(43) Lewin, A.; Moore, G. R.; Le Brun, N. E. *Dalton Trans.* **2005**, *22*, 3597–3610.

The Mössbauer spectra were obtained using an Austin S-600 Mössbauer spectrometer with a conventional constant accelerated driver and a 70 mCi Co^{57} in a Rh matrix source. The spectrometer was calibrated using α-Fe foil, and the isomer shift was calibrated using an α-Fe foil at room temperature. Spectra were collected on 10 films deposited on highly oriented pyrolyphic graphite (HOPG) at four different potentials. The film and an underlying HOPG layer were removed with tape. For every deposit, the HOPG was cleaned with hydrochloric acid to remove the previous deposition, then rinsed with water. A fresh surface of HOPG was prepared by removing the surface layers with tape. Analysis of the measured spectra was performed using a least-squares program.

An X-ray analysis of each film was preformed using a high-resolution Philips X-Pert MRD X-ray diffractometer with a Cu Kα1 radiation source (λ = 0.154056 nm). The symmetric X-ray diffraction patterns were obtained using the line focus mode. The primary optics of a combination Göbel mirror and a two crystal Ge(220) two-bounce hybrid monochromator (PW3147/00) producing pure $CuK\alpha_1$ radiation on the incident beam side. A 0.18° parallel plate collimator (PW3098/18) was used as the secondary (diffracted beam) optics. Scans were run from 2θ values of 10° to 100°. The lattice parameter of each film was determined by Reitveld analysis using RIQAS software from Materials Data Inc.

The in-plane orientation of the films relative to the Au single crystal was determined by X-ray pole figures and azimuthal scans. For these measurements of the epitaxial films, the diffractometer was operated in the point focus mode with a crossed slit collimator module (PW3084/62) as the primary optics. A 0.27° parallel plate collimator (PW3098/27) equipped with a flat graphite monochromator (PW3121/00) was used as the secondary optics. To perform the pole figure analysis, the 2θ was set to the angle of the $Fe_3O_4(311)$ plane (2θ = 35.426°) and the $Fe_{10}O_{14}(OH)_2(11\bar{2}0)$ plane (2θ = 35.04°) for the films analyses and to that of the Au(311) plane (2θ = 77.547°) for the substrate analyses. The sample was moved through a sequence of tilt angles, χ, from 0° to 90°, and at each χ, the sample was rotated azimuthally, ϕ, from 0° to 360°. Data were collected in the continuous mode over 3° intervals for both χ and ϕ, with a count time of 5 seconds per point. Azimuthal scans were performed under the same conditions but using χ = 58.5° for the films on Au(111) and Au(100) and χ = 31.5° for the films on Au(110). Following the X-ray diffraction analyses, the film morphologies were studied using an Hitachi S-4700 field emission scanning electron microscope.

Results and Discussion

Figure 1 shows linear sweep voltammograms on a gold rotating disk electrode at 100 rpm in an alkaline TEA bath (blue squares) and the alkaline Fe(III)−TEA deposition bath (black solid line) at 80 °C. From their open circuit potentials of −0.41 V for the TEA bath and −0.47 V for the Fe(III)—TEA bath, they are scanned at 50 mV/s to −1.400 V vs Ag/AgCl. The linear sweep voltammogram of 0.1 M TEA in 2 M NaOH (Figure 1, blue squares) shows that the alkaline TEA is electrochemically inactive and that the electrochemical generation of hydrogen gas begins around −1.25 V vs Ag/AgCl. The electrochemical reduction of the alkaline Fe(III)−TEA (Figure 1, black solid line) is apparent at potentials more negative than −0.950 V vs Ag/AgCl. The initial stage of this linear

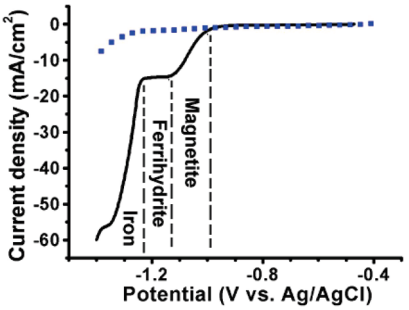

Figure 1. The linear sweep voltammograms of an alkaline TEA solution (blue squares) and Fe(III)−TEA solution (black solid line) at 80 °C scanned at 50 mV/s at a rotation of 100 rpm on a gold rotating disk electrode. The alkaline TEA solution consisted of 0.1 M TEA in 2 M NaOH. The alkaline Fe(III)−TEA solution consisted of 43 mM $Fe_2SO_4 \cdot nH_2O$, 0.1 M TEA, and 2 M NaOH.

sweep is a one-electron reaction in which an Fe(III) species is reduced to an Fe(II) species. Black films are produced from −1.01 to −1.09 V vs Ag/AgCl. At more negative deposition potentials, the electrodeposited films are green. They become black and reddish brown as they dry in air. When the potential becomes more negative than −1.23 V vs Ag/AgCl, a two-electron process occurs as the Fe(II) is reduced to Fe. Gray films are produced at −1.3 V vs Ag/AgCl. The competing reaction of hydrogen evolution continues as the potential becomes more negative. The potential range for electrodepositing each material is shown in Figure 1.

The surface concentration of Fe(III) is dependent on the departure from equilibrium. At low overpotentials, the Fe(III) surface concentration is nearly the same as the bulk concentration, whereas at high overpotentials, at which the current becomes mass-transport controlled, the surface concentration of Fe(III) approaches zero. As a result, magnetite films grown at low overpotentials would be nonstoichiometric and rich in Fe(III), whereas films grown at high overpotentials would be nonstoichiometric and rich in Fe(II). Electrochemical studies using cyclic voltammetry have shown that the reduction of Fe(III)−TEA complexes is a one-electron process in which an Fe(III)—TEA complex is reduced to an Fe(II)−TEA complex.[44−48] Using reported stability constants of iron−triethanolamine complexes,[49,50] this reduction may occur as expressed in eq 1. Other studies have suggested complexes with a Fe(III) to TEA ratio of 1:1 and a hydroxide coordination number which depends on pH, but their stability constants have not been determined.[44,47,51] The Fe(III)−TEA complex then chemically reacts with the Fe(II)−TEA to produce magnetite (eq 2).

(44) Mohr, S.; Bechtold, T. *J. Appl. Electrochem.* **2001**, *31*, 363.
(45) Wen, Y. H.; Zhanag, H. M.; Qian, P.; Zhou, H. T.; Zhao, P.; Yi, B. L.; Yang, Y. S. *Electrochim. Acta* **2006**, *51*, 3769.
(46) Bechtold, T.; Burtscher, E.; Amann, A.; Bobleter, O. *J. Chem. Soc., Faraday Trans.* **1993**, *89*, 169.
(47) Ibanez, J. G.; Choi, C.; Becker, R. S. *J. Electrochem. Soc.* **1987**, *134*, 8.
(48) Thomas, B.; Aurora, T. *J. Electroanal. Chem.* **2005**, *580*, 173.
(49) Sillén, , L. G. *Stability Constants of Metal-Ion Complexes;* Chemical Society: London, 1971; Suppl. 1.
(50) Perrin, D. D. *IUPAC Stability Constants of Metal-Ion Complexes: Part B Organic Ligands*. Pergamon Press: New York, 1979.
(51) Polcyn, D. S.; Shain, I. *Anal. Chem.* **1966**, *38*, 376.

Table 1. Potentials and Constants Used to Calculate the Potential for the Reduction of $Fe(OH)_4TEA_2^-$ to Fe_3O_4

equations	constant at 25 °C	reference
$Fe(OH)_4TEA_2^- \leftrightarrows Fe^{3+} + 2TEA + 4OH^-$	$K = 10^{-44.6}$	50
$Fe^{3+} + e^- \leftrightarrows Fe^{2+}$	$E^o = 0.771$ V vs NHE	54
$Fe^{2+} + 2TEA \leftrightarrows FeTEA_2^{2+}$	$K = 10^{3.59}$ (49)	49
$Fe(OH)_4TEA_2^- + e^- \leftrightarrows Fe(TEA)_2^{2+} + 4OH^-$	$E^o = -1.65$ V vs NHE	calcd
$2Fe(OH)_4TEA_2^- + Fe(TEA)_2^{2+} \leftrightarrows Fe_3O_4 + 6TEA + 4H_2O$	$\Delta G_{rxn} = -87.82$ kJ/mol	calcd
species	ΔG_f^o	
TEA	−315.6 kJ/mol	52
Fe^{2+}	−78.87 kJ/mol	53
Fe^{3+}	−4.7 kJ/mol	53
OH^-	−157.293 kJ/mol	54
$Fe(OH)_4TEA_2^-$	−1519.64 kJ/mol	calcd
Fe_3O_4	−1015.5 kJ/mol	53
H_2O	−237.14 kJ/mol	54
$FeTEA_2^{2+}$	−730.56 kJ/mol	calcd

Equation 3 is the overall electrochemical−chemical reaction for magnetite deposition from this solution.

$$Fe(OH)_4TEA_2^- + e^- \leftrightarrows Fe(TEA)_2^{2+} + 4OH^- \quad (1)$$

$$2Fe(OH)_4TEA_2^- + Fe(TEA)_2^{2+} \leftrightarrows Fe_3O_4 + 6TEA + 4H_2O \quad (2)$$

$$3Fe(OH)_4TEA_2^- + e^- \leftrightarrows Fe_3O_4 + 6TEA + 4H_2O + 4OH^- \quad (3)$$

The E^o of the overall reaction in eq 3 is calculated to be −0.745 V vs NHE (−0.944 V vs Ag/AgCl) at room temperature. This calculation is based on the equations and constants found in Table 1.[49,50,52−54] Assuming that the [TEA] = 0.1 M and the $[Fe(OH)_4TEA_2^-]$ = 0.05 M at a pH of 14, the E is calculated to be −0.869 V vs NHE (−1.068 V vs Ag/AgCl). Although this value is calculated at 25°C, it is close to the $E_{1/2}$ of −1.062 V vs Ag/AgCl at 80 °C from the linear sweep voltammogram in Figure 1.

The X-ray diffraction patterns of the black films deposited by applying potentials from −1.01 V to −1.09 V vs Ag/AgCl were consistent with magnetite. All these films were crystalline, as shown in the XRD patterns of films deposited on stainless steel at −1.01 V vs Ag/ACl (Figure 2A) and −1.05 V vs Ag/AgCl (Figure 2B). As the deposition potential becomes more negative, the lattice parameter of the magnetite decreases. The magnetite films deposited at −1.01 V vs Ag/AgCl have no preferred orientation (a = 0.8423 nm), whereas those deposited at −1.05 V vs Ag/AgCl show a strong [100] preferred orientation (a = 0.8394 nm). The X-ray diffraction patterns of black and reddish brown films deposited at −1.10 V vs Ag/AgCl, shown in Figure 2C, showed two main peaks that can be identified as (311) and (440) peaks of magnetite. The X-ray diffraction patterns of the reddish brown films deposited at −1.20 V vs Ag/AgCl (not shown) are similar to those of films deposited at −1.10 V vs Ag/AgCl. The gray films deposited at −1.30 V vs Ag/AgCl are consistent with body centered cubic iron (Figure 2D). Other than the substrate peaks, no other peaks were present in the XRD patterns.

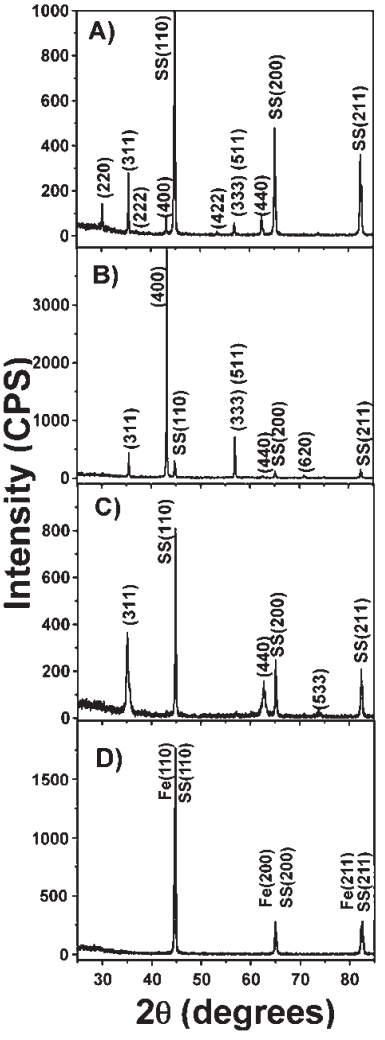

Figure 2. Symmetric X-ray diffraction patterns of magnetite films deposited on 430 stainless steel substrates at a potential of (A) −1.01, (B) −1.05, (C) −1.10, and (D) −1.30 V vs Ag/AgCl until 1 C/cm^2 was passed at 80 °C.

The morphology of the film changes as the applied reduction potential is changed. The SEM images in

(52) Frings, J.; Wondrak, C.; Schink, B. *Ach. Microbiol.* **1994**, *162*, 103.
(53) Bard, A. J.; Parsons, R.; Jordan, J. *Standard Potentials in Aqueous Solution*. Marcel Dekker: New York, 1985.
(54) Lide, D. R. *CRC Handbook of Chemistry and Physics*, 77th ed.; CRC Press: New York, 1996.

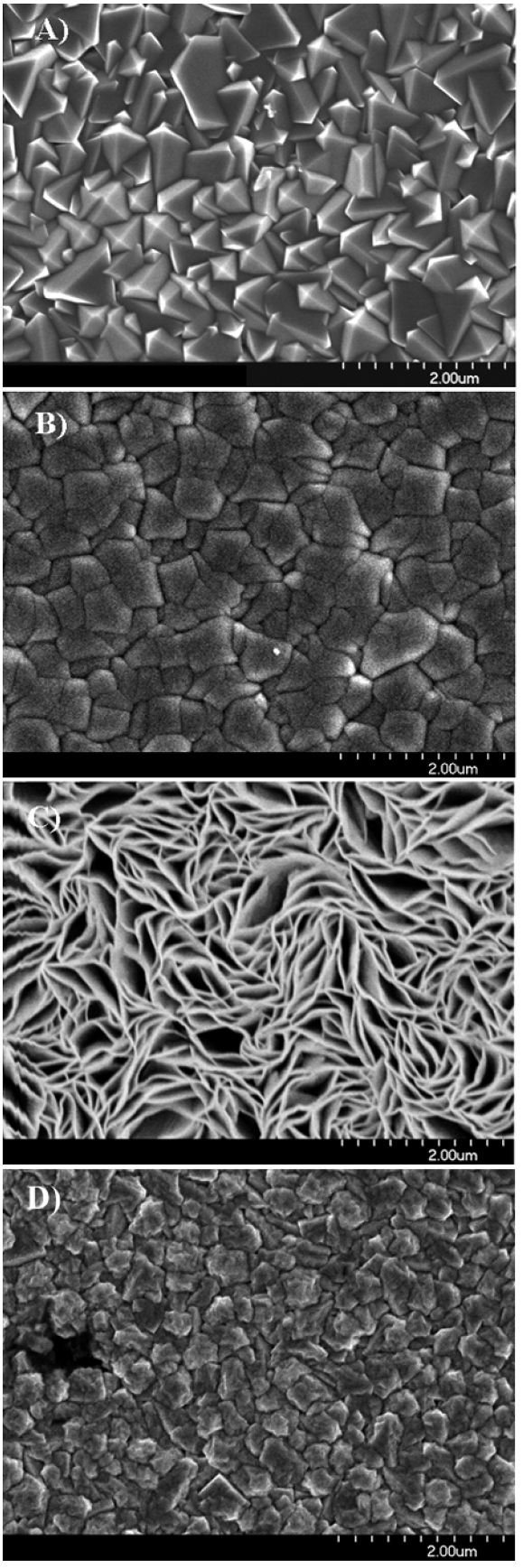

Figure 3. SEM images of films deposited on stainless steel at (A) −1.01, (B) −1.05, (C) −1.10, and (D) −1.30 V vs Ag/AgCl. The films were deposited at 80 °C until 1 C/cm^2 passed.

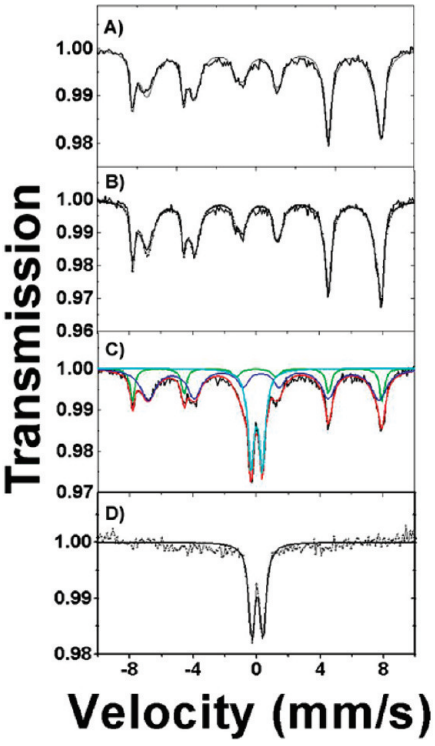

Figure 4. Room temperature Mössbauer spectra of films deposited on HOPG at (A) −1.01, (B) −1.05, (C) −1.10, and (D) −1.20 V vs Ag/AgCl. Spectra A and B are composed of two sets of sextets consistent with magnetite. Spectrum C shows two sextets and a doublet associated with magnetite and ferrihydrite, respectively. Spectrum D shows a ferrihydrite doublet.

Figure 3 show the effect of potential on the surface morphology of the materials on stainless steel. The magnetite films grown at lower overpotentials have highly faceted, dense morphologies, as shown in the SEM image of a film deposited on stainless steel by applying −1.01 V vs Ag/AgCl (Figure 3A). In Figure 3B, films deposited at −1.05 V vs Ag/AgCl are featureless, yet dense. The films grown in the mass-transport limited region between −1.10 and −1.20 V vs Ag/AgCl have ribbon-like microstructures, as seen in Figure 3C. The iron films grown at −1.30 V vs Ag/AgCl revert to a featureless, dense morphology (Figure 4).

To determine the phases and stoichiometry of the films, Mössbauer spectroscopy was performed on films deposited at four different potentials on HOPG. Figure 4 and Table 2 show the room temperature Mössbauer spectra and corresponding parameters of films deposited at (A) −1.01, (B) −1.05, (C) −1.10, and (D) −1.20 V vs Ag/AgCl. A single phase exists in films in which −1.01 and −1.05 V vs Ag/AgCl were applied (Figure 4A,B). These spectra were fit with two Lorentzian sextets, which provide the intensity values from the tetrahedral sites (Fe^{3+}) and from the octahedral sites (Fe^{2+}, Fe^{3+}). The spectra indicate that the final products are nonstoichiometric magnetite. Of the two, the films deposited at −1.05 V vs Ag/AgCl are closer to stoichiometric magnetite than the film deposited at −1.01 V vs Ag/AgCl. These films have a higher Fe(III) concentration than found in stoichiometric magnetite. Consistent with the earlier discussion, the

Table 2. The Mössbauer Spectral Parameters at 25 °C Obtained from the Spectra in Figure 4 of Films Deposited from Four Different Potentials vs Ag/AgCl. The Isomer Shifts Are Given Relative to the α-Fe Foil at 25 °C

potential (V)	compound	component	IS (mm/s)	QS (mm/s)	HF (kOe)	ratio (%)
−1.01	magnetite	Fe(3+)	0.3390	0.0878	488.87	26.51
		Fe(2+ and 3+)	0.6820	0.0732	453.53	73.49
−1.05	magnetite	Fe(3+)	0.3169	0.0768	488.22	28.78
		Fe(2+ and 3+)	0.6645	0.0815	452.92	71.22
−1.10	magnetite	Fe(3+)	0.3157	0.0622	489.80	17.13
		Fe(2+ and 3+)	0.6716	0.1465	453.66	52.69
	ferrihydrite		0.3091	0.7186		30.19
−1.20	ferrihydrite		0.3291	0.7451		100

surface concentration of electrochemically generated Fe(II) at these potentials is insufficient to produce stoichiometric magnetite films. In Figure 4C, an applied potential of −1.10 V produced films with two phases. This spectrum was fit with a doublet shown in green and two Lorentzian sextets: tetrahedral sites (Fe^{3+}) shown in red and octahedral sites (Fe^{2+} and Fe^{3+}) shown in blue. About 70% of the film is nonstoichiometric magnetite represented by the two sextets. The quadrupole splitting of the doublet for this film is 0.72 mm/s. Since most Fe(III) oxides produce a doublet with a quadrupole splitting of 0.5−0.6 mm/s in the Mössbauer spectra, the remaining 30% of this film is determined to be ferrihydrite, consistent with the reported quadrupole split doublet of paramagnetic ferrihydrite (0.7−0.85 mm/s).[1,37] In Figure 4D, the Mössbauer spectrum of films deposited at −1.20 V vs Ag/AgCl shows just a doublet (QS = 0.75 mm/s), indicating that only ferrihydrite is present.

The production of ferrihydrite, an Fe(III) compound, is unexpected since it is produced at more negative potentials at which the surface concentration of Fe(II) is high. Films deposited at −1.10 and −1.20 V vs Ag/AgCl are initially green; they then air oxidize to black, then reddish brown films. The green film is consistent with the production of green rust (GR). Green rust is a mixed iron(II)−iron(III) hydroxide containing an anion such as chloride, sulfate, or carbonate. For this study, sulfate green rust ($Fe_4^{II}Fe_2^{III}(OH)_{12}SO_4{*}nH_2O$) would be feasible. SEM images of sulfate GR resembling those found in Figure 3C have been electrodeposited from a slightly basic Fe(II)−sulfate solution at 25 °C.[55,56] However, the Mössbauer spectra of the film deposited at −1.10 and −1.20 V vs Ag/AgCl (shown in Figure 4C,D) show no indication of GR.[57−61] However, the conversion of sulfate GR to magnetite has been reported.[55,60−62] Cellular structures of magnetite, similar to those seen in Figure 3C, have been produced by the chemical oxidation of electrodeposited sulfate GR films using 0.1 M NaOH at 70 °C.[62] One study has also shown that the aerial oxidation of $Fe(OH)_2$ in basic medium produces GR, which is converted to magnetite and ferrihydrite.[61] The adsorption of anions stabilizes ferrihydrite and hinders further oxidation to more stable iron hydroxides or oxides.[1,37,61,63] Therefore, the broadening of the film peaks in the XRD pattern in Figure 2C may be attributed to two-line ferrihydrite. The two film peaks can be indexed as $(11\bar{2}0)$ at 35.04° and $(30\bar{3}0)$ at 62.69° for a two-line ferrihydrite film using JCPDS no. 29-712. Therefore, the production of ferrihydrite at these potentials is consistent with the aerial oxidation of an electrodeposited GR film in basic conditions.

On the basis of the cross-sectional SEM images of the films deposited on Au on glass, the nonstoichiometric magnetite films were found to deposit at −1.01 V vs Ag/AgCl deposit with a current efficiency of 45% (2.1 μm for 1 C/cm^2), whereas the nonstoichiometric magnetite films deposited at −1.05 V vs Ag/AgCl deposit with a current efficiency of 48% (2.2 μm for 1 C/cm^2). The low current efficiency for the magnetite deposition at the potentials investigated suggests that another reaction is occurring that is either contributing to the measured current or inhibiting film growth, or that dissolution of the films is competing with deposition of the film. Two layers are visible in the cross-sectional SEM images of a film deposited at −1.10 V vs Ag/AgCl for 1C/cm^2, whereas one layer is observed for a film deposited at −1.20 V vs Ag/Cl. These observations are consistent with the Mössbauer results in Figure 4. Deposited at −1.10 V vs Ag/AgCl, the thickness of the porous upper layer of ferrihydrite is 2.8 μm while the underlying magnetite film has a current efficiency of 43% (2.0 μm for 1 C/cm^2). The ferrihydrite films deposited at −1.20 V vs Ag/AgCl for 1 C/cm^2 have a porous film thickness of 4.3 μm.

Films were then deposited at −1.01, −1.05, −1.10, and −1.20 V vs Ag/AgCl on Au(111), Au(001), and Au(110) for epitaxial studies. An epitaxial film has out-of-plane and in-plane orientation. To determine the out-of-plane orientations of the films, symmetric-scan X-ray diffraction patterns were used. Figure 5 shows X-ray diffraction patterns of magnetite films deposited at a potential of −1.01 V vs Ag/AgCl on gold single crystals. On Au(111) and Au(001), (111)-type peaks of Fe_3O_4 were detected as

(55) Antony, H.; Legrand, L.; Chausse, A. *Electrochim. Acta* **2008**, *53*, 7146.
(56) Antony, H.; Labrit, A.; Rouchaud, J. C.; Legrand, L.; Chausse, A. *Electrochim. Acta* **2008**, *53*, 7173.
(57) Ruby, C.; Aissa, R.; Gehin, A.; Cortot, J.; Abdelmoula, M.; Genin, J.-M. *C. R. Geosci.* **2006**, *338*, 420.
(58) Genin, J.-M. R.; Refait, P.; Bourrie, G.; Abdelmoula, M.; Trolad, F. *Appl. Geochem.* **2001**, *16*, 559.
(59) Genin, J.-M. R.; Abdelmoula, M.; Aissa, R.; Ruby, C. *Hyperfine Interact.* **2005**, *166*, 391.
(60) Ruby, C.; Gehin, A.; Aissa, R.; Genin, J.-M. R. *Corrosion Sci.* **2006**, *48*, 3824.
(61) Genin, J.-M. R.; Ruby, C.; Gehin, A.; Refait, P. *C. R. Geosci.* **2006**, *338*, 433.
(62) Chung, K. W.; Kim, K. B.; Han, S.-H.; Lee, H. *Electrochem. Solid State Lett.* **2005**, *8*, A259.
(63) Furukawa, Y.; Kim, J.-W.; Watkins, J.; Wilkens, R. T. *Environ. Sci. Technol.* **2002**, *36*, 5469.

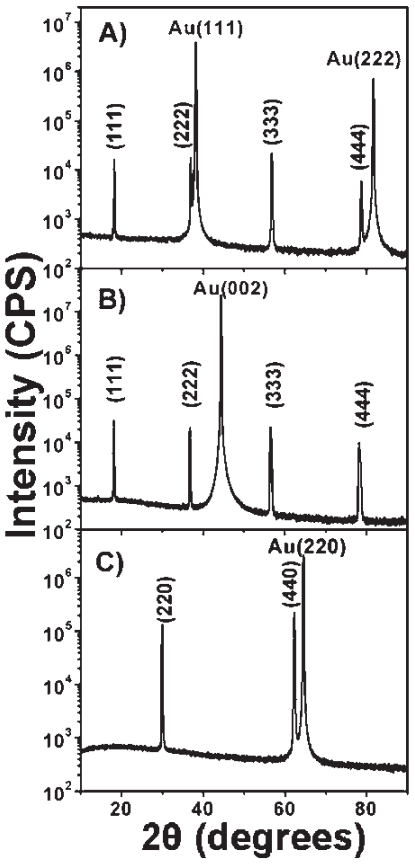

Figure 5. X-ray diffraction patterns of magnetite deposited on (A) Au-(111), (B) Au(001), and (C) Au(110) for 300 s at −1.01 V vs Ag/AgCl at 80 °C. Magnetite films deposited on Au(111) and Au(001) are (111) oriented, whereas films deposited on Au(110) are (110) oriented.

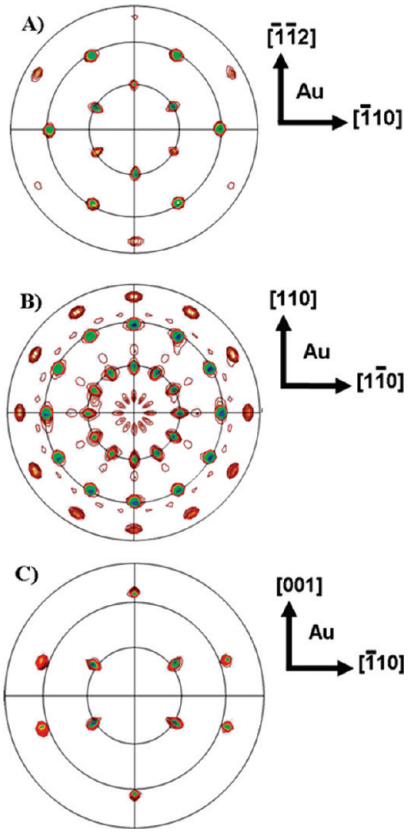

Figure 6. The (311) pole figures of magnetite films deposited on (A) Au(111), (B) Au(001), and (C) Au(110) for 300 s at −1.01 V vs Ag/AgCl at 80 °C. The radial grid lines on the pole figure correspond to 30° increments of the tilt angle, χ.

seen in Figure 5 panels A and B, respectively. On Au(110), only the (220) and (440) peaks for Fe_3O_4 were observed as shown in Figure 5C. No other peaks are present in the diffraction patterns. Therefore, thin films of magnetite on Au(111) and Au(001) grow with a [111] out-of-plane orientation, whereas the film on Au(110) grows with a [110] out-of-plane orientation.

The in-plane orientations of the films were determined by X-ray pole figures. Since a polycrystalline film has no out-of-plane or in-plane orientation, a pole figure of a polycrystalline film would have uniform intensity. In the pole figure, a film with fiber texture results in a ring pattern, whereas an epitaxial film has distinct peaks. Figure 6 shows the (311) pole figures of Fe_3O_4 films on gold single crystals deposited at −1.01 V vs Ag/AgCl. Figure 6A shows the (311) pole figure from an Fe_3O_4 film deposited on Au(111) with six reflections at azimuthal angles, χ, at 29.5°, 58.5°, and 80°. The presence of six peaks in the pole figure at 29.5° and 80° indicates two {111} domains of Fe_3O_4 rotated 180° on Au(111). One set of the three reflections is more intense than the other three. A pole figure of a magnetite film on Au(001) in Figure 6B reveals in-plane [111] and [511] orientations. The presence of [511] orientations is common because of the twinning of the {111} planes.[5] Since the (333) and (511) planes have the same d-spacing, the presence of the (511) is difficult to verify by examining an X-ray diffraction pattern. The clearest indication of the presence of the (511) orientation is in pole figures. When running a (311) pole figure, the {311} reflections related to the [511] orientation have χ's equal to 9.5°, 29.5°, 41°, 58.5°, 66°, 80°, and 86.7°. Some of these χ's coincide with χ's of the reflections due to [111] orientation. The number of (511) domains was determined using χ = 9.5°, since a single domain of (511) has one peak at this χ. Therefore, the epitaxial magnetite film on Au(001) in Figure 6B has 4 domains of the three-fold symmetric [111] orientation as well 12 domains of the [511] orientation. Pole figures and XRD patterns of magnetite films deposited on Au(001) at −1.01 V vs Ag/AgCl for more than 1 C/cm^2 have shown that these epitaxial films grow with [111], [511], and [001] orientations. The pole figure analysis of Figure 6C for a film on Au(110) is simpler. The angles between {311} and {110} planes are 31.5°, 64.8°, and 90°. This pole figure is consistent with a single domain [110] in-plane orientation of Fe_3O_4 on Au(110).

In conjunction with the pole figures and stereographic projections of the films and substrate, azimuthal scans were used to determine the epitaxial relationships. An epitaxial relationship describes how the film is oriented relative to the substrate by finding a direction of the film parallel to a direction in the substrate. Evident in the azimuthal scans in Figure 7A,B, the main {111} Fe_3O_4 domain on the Au(111) aligns antiparallel to the substrate, whereas the four {111} Fe_3O_4 domains are

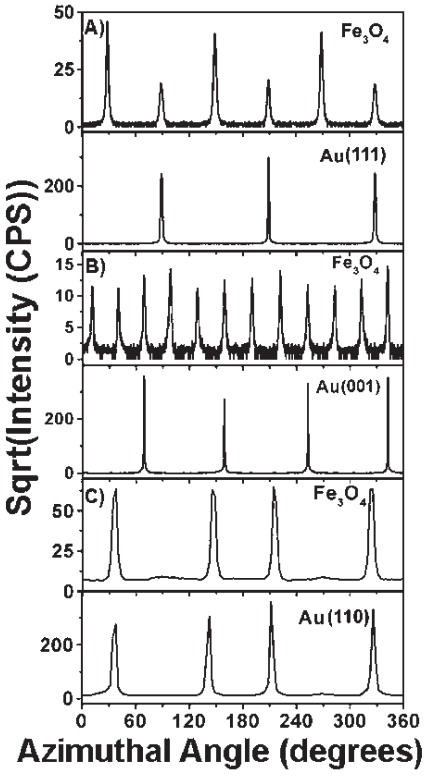

Figure 7. The (311) azimuthal scans of magnetite and gold for magnetite films deposited on (A) Au(111), (B) Au(001), and (C) Au(110). For each set of azimuthal scans, the top plot is the magnetite azimuthal scan and the bottom plot is the substrate azimuthal scan.

equivalent on Au(001). For the magnetite films on Au(111), the epitaxial relationships can be expressed as $Fe_3O_4(111)[01\bar{1}]//Au(111)[0\bar{1}1]$ for the antiparallel domain and $Fe_3O_4(111)[0\bar{1}1]//Au(111)[0\bar{1}1]$ for the parallel domain. That is, for the dominate domain (antiparallel), the $Fe_3O_4(111)$ and Au(111) planes are parallel and the $Fe_3O_4[01\bar{1}]$ and $Au[0\bar{1}1]$ in-plane directions are coincident. Similarly, for the parallel domain, the $Fe_3O_4(111)$ and Au(111) planes are parallel but the $Fe_3O_4[0\bar{1}1]$ and $Au[0\bar{1}1]$ in-plane directions are coincident. The epitaxial relationships for the four Fe_3O_4 domains on Au(001) are $Fe_3O_4(111)[0\bar{1}1]//Au(001)[110]$, $Fe_3O_4(111)[0\bar{1}1]//Au(001)[1\bar{1}0]$, $Fe_3O_4(111)[0\bar{1}1]//Au(001)[\bar{1}10]$, and $Fe_3O_4(111)[0\bar{1}1]//Au(001)[\bar{1}10]$. For each of these four relationships, three arrangements exist owing to the (511) orientation: $(511)[\bar{2}55]$, $(511)[\bar{1}14]$, and $(511)[\bar{1}41]$. Figure 7C shows that the [110] oriented magnetite film has one domain and is aligned on the Au(110). Therefore, the epitaxial relationship for the (110) magnetite films on Au(110) is $Fe_3O_4(110)[001]//Au(110)[001]$. Thin magnetite films deposited at the more negative potentials of −1.05 V vs Ag/AgCl produced the same out-of-plane and in-plane orientations although the films were deposited at a different potential (not shown).

The SEM images of magnetite on the gold single crystals deposited at −1.01 V vs Ag/AgCl are shown in Figure 8. Consistent with the pole figure and azimuthal scan analysis of a film on Au(111), the micrograph in Figure 8A reveals two sets of [111] triangular facets rotated 180° with respect to each other. The majority of

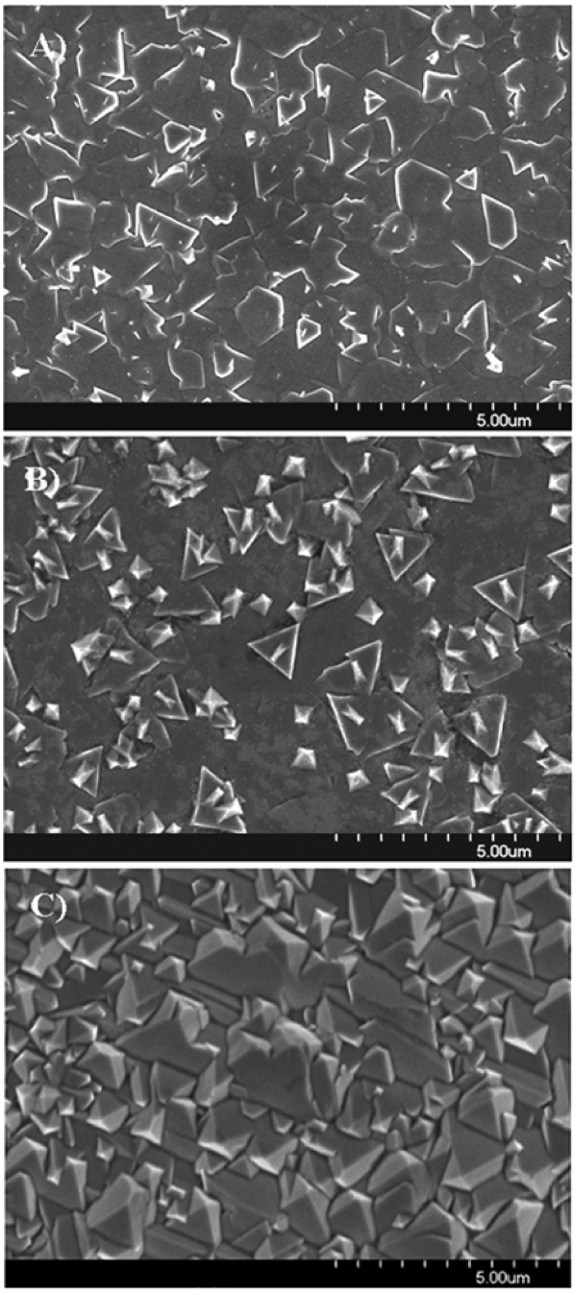

Figure 8. SEM images of magnetite deposited on (A) Au(111), (B) Au(001), and (C) Au(110) for 300 s at −1.01 V vs Ag/AgCl at 80 °C.

the facets point upwards and to the left. Figure 8B shows similar underlying [111] triangular facets pointing in four directions on Au(001). On these facets are elongated pyramids attributed to the [511] orientation from the twinning of the {111} facets. Figure 8C shows pyramidal crystallites that indicate an underlying [110] orientation.

The X-ray diffraction patterns of the film grown at −1.10 and −1.20 V vs Ag/AgCl on Au(110) are shown in Figure 9A,B, respectively. The film deposited at −1.10 V vs Ag/AgCl has two out-of-plane orientations: [110] oriented magnetite and $(11\bar{2}0)$ oriented ferrihydrite. The SEM images in Figure 10 show the morphologies of the film deposited at −1.10 V vs Ag/AgCl on Au(110). Figure 10A shows an area where two morphologies are present, and the nanoribbon morphology seems to grow

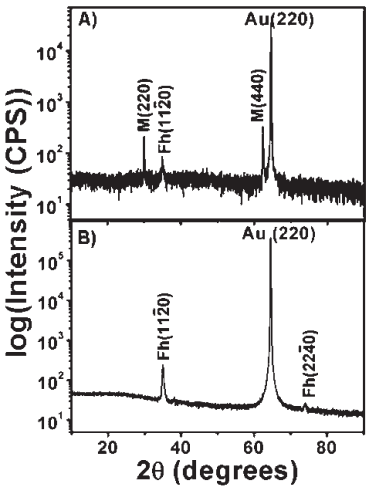

Figure 9. X-ray diffraction patterns of magnetite and ferrihydrite electrodeposited at (A) −1.10 and (B) −1.20 V vs Ag/AgCl on Au(110). M indicates a peak assigned to a magnetite plane, whereas Fh indicates a peak assigned to a ferrihydrite plane.

along the grain boundaries of the underlying material. Figure 10B shows the ribbonlike morphology that covers the surface. These ribbons are 20−30 nm wide. Figure 10C shows the morphology of the underlying film. Films deposited at −1.10 V vs Ag/AgCl on Au(001) and Au(111) have similar morphologies (not shown). The films deposited at a more negative potential of −1.20 V vs Ag/AgCl have similar ribbon morphologies, yet the X-ray diffraction pattern (Figure 9B) and Mossbauer spectrum (Figure 4D) do not indicate the presence of magnetite. In the X-ray diffraction pattern of the film deposited at −1.20 V vs Ag/AgCl on Au(110), only the (11$\bar{2}$0) and (22$\bar{4}$0) peaks of ferrihydrite are present (Figure 9B). Since only ferrihydrite is detected for the films deposited at −1.20 V vs Ag/AgCl, the ribbon morphology is attributed to the ferrihydrite. Therefore, the SEM image in Figure 10C shows the morphology of the magnetite film under the ribboned ferrihydrite seen in Figure 10B. A cross-sectional SEM image of a film deposited at −1.10 V vs Ag/AgCl on Au on glass for 1C/cm^2 is shown in Figure 10D. In this figure, the thickness of the porous, ferrihydrite platelet is 2.8 μm, whereas the lower magnetite columns grew to a thickness of 2.0 μm.

The (311) magnetite pole figures for films deposited at −1.10 V and −1.20 V vs Ag/AgCl on Au(110) are shown in Figures 11A,B, respectively. The d-spacing of magnetite (311) is very close to the d-spacing of ferrihydrite (11$\bar{2}$0), which results in the reflection of ferrihydrite (11$\bar{2}$0) peaks in the same pole figure. Similarly, the d-spacing of magnetite (311) is near the d-spacing of Au(111). For the thin films, therefore, {111} reflections from the Au(110) planes are also evident in the same pole figure. Although the 2θ is maximized to observe the reflection from the magnetite (311) planes, the final pole figure is actually a superposition of the magnetite (311), ferrihydrite (11$\bar{2}$0), and Au(111) pole figures.

For a film deposited at −1.10 V vs Ag/AgCl, the pole figure in Figure 11A is consistent with one domain of

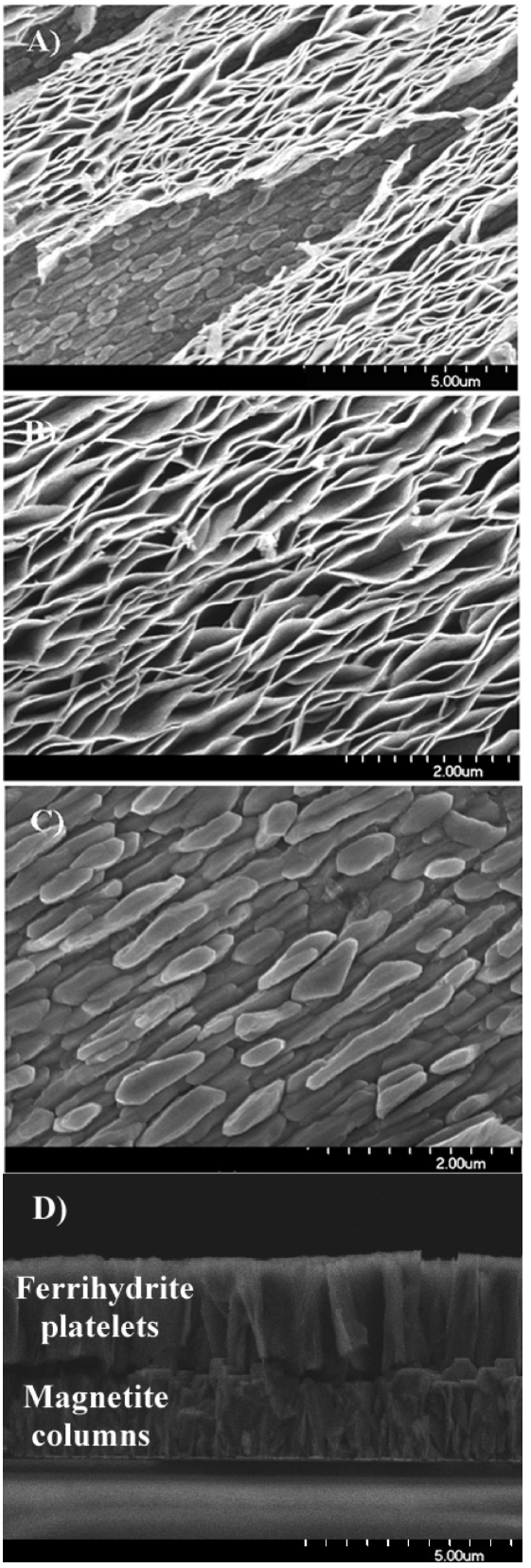

Figure 10. SEM images of a film deposited at −1.1 V vs Ag/AgCl at 80 °C on Au(110). (A) SEM image of the overall view of the surface of the film, showing two distinct morphologies. The ribbonlike morphology of ferrihydrite (B) on underlying nonstoichometric magnetite (C) is shown. (D) Cross-sectional SEM image of a film deposited at −1.1 V vs Ag/AgCl on Au on glass. The thickness of the ferrrihydrite platelets is 2.8 μm (upper layer), whereas the thickness of the magnetite columns is 2.0 μm (lower layer).

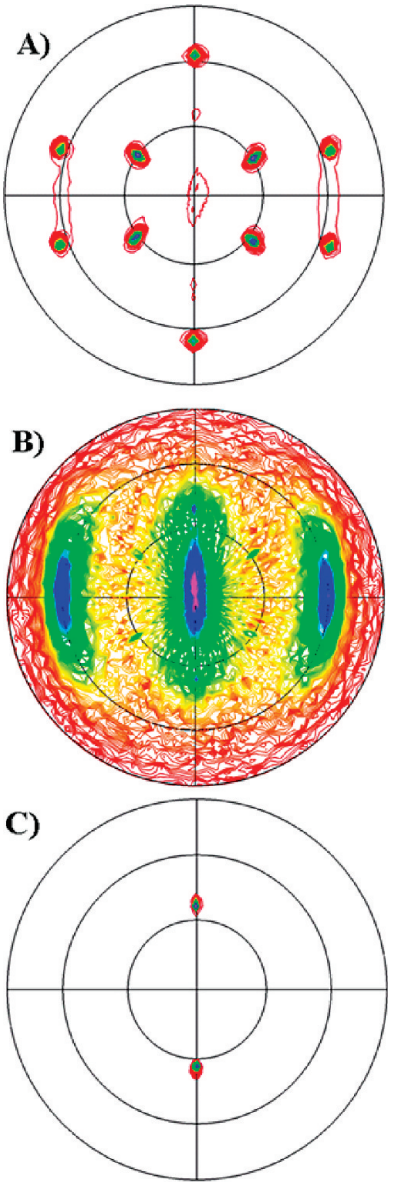

Figure 11. The (311) magnetite pole figures of (11$\bar{2}$0) ferrrihydrite on (110) magnetite on Au(110) electrodeposited at (A) −1.10 and (B) −1.20 V vs Ag/AgCl. The (311) magnetite pole figure is actually probing three planes: (311) magnetite, (11$\bar{2}$0) ferrihydrite, and (111) Au due to their similar d-spacings. Figure C is a (111) Au pole figure of the Au(110) substrate. The radial grid lines on the pole figure correspond to 30° increments of the tilt angle, χ.

magnetite with a [110] in-plane orientation on Au(110). In addition to these {311} reflections of [110] oriented magnetite in Figure 11A, three low intensity, broad peaks at $\chi = 0°$ and $\chi = 60°$ (180° apart) are present in the pole figure. These peaks cannot be explained by a (311) reflection of any orientation of Fe_3O_4.

As seen in the XRD pattern in Figure 9A, magnetite and ferrihydrite are present in this film deposited at −1.10 V vs Ag/AgCl. The X-ray diffraction pattern in Figure 9B indicates that the film deposited at −1.20 V vs Ag/AgCl was (11$\bar{2}$0) oriented ferrihydrite on Au(110). A pole figure of this film was run to determine if the broad peaks were due to an epitaxial (11$\bar{2}$0) ferrihydrite film. This pole figure, shown in Figure 11B, has higher intensity peaks with azimuthal FWHM of 46° at $\chi = 0°$ and 60°, the same χ of the broad peaks seen in Figure 11A. The nanoribbon morphology of the ferrihydrite causes the anisotropy observed in the pole figure shown in Figure 11A,B. This phenomenon can be explained by reexamining SEM images of ferrihydride, such as Figure 10B. As the ferrihydrite nanoribbons begin their growth at the magnetite grain boundaries, the resulting electrodeposit is not compact. This loose packing manifests itself in the wavy appearance of the nanoribbons seen in Figure 10B, as well as in the anisotropic character of the pole figure in Figure 11B.

The broad peaks in Figure 11B are assigned to the {11$\bar{2}$0} reflections of (11$\bar{2}$0) oriented ferrihydrite. Although the X-ray diffraction pattern of the film deposited at −1.20 V vs Ag/AgCl in Figure 9B shows no magnetite, the pole figure does indicate that an [110] oriented magnetite film is present by the four weak {311} reflections of magnetite (111) at $\chi = 30°$. The two additional sharp peaks at $\chi = 35°$, 180° apart, are {111} reflections of Au owing to the Au(110) in Figure 11A,B. The Au(111) pole figure for the Au(110) substrate is shown in Figure 11C to confirm the location of the Au reflections in these pole figures. On the basis of the pole figure analyses, the epitaxial relationship for the two films on Au(110) are determined to be $Fe_{10}O_{14}(OH)_2$)(11$\bar{2}$0)-[0001]//Fe_3O_4(110)[001]//Au(110)[001]. The epitaxial relationships for the films deposited on Au(001) and Au(111) are $Fe_{10}O_{14}(OH)_2$)(11$\bar{2}$0)[0001]//Fe_3O_4(001)-[110]//Au(001)[110], $Fe_{10}O_{14}(OH)_2$)(11$\bar{2}$0)[$\bar{1}$100]//Fe_3O_4-(001)[110]//Au(001)[110], and $Fe_{10}O_{14}(OH)_2$)((11$\bar{2}$0)-[$\bar{1}$100]//Fe_3O_4(111)[01$\bar{1}$]//Au(001)[01$\bar{1}$].

Conclusion

Varying the reduction potential permits the deposition of magnetite, ferrihydrite, and iron from the Fe(III)−TEA deposition bath. Magnetite films are deposited at potentials from −1.01 to −1.10 V vs Ag/AgCl. Ferrihydrite films are deposited at the potentials of −1.10 and −1.20 V vs Ag/AgCl, whereas iron films are deposited at more negative potentials. The magnetite and ferrihydrite films are epitaxial on gold single crystals. Magnetite deposited on Au(111) and Au(001) is [111] oriented, whereas magnetite on Au(110) is [110] oriented. Films deposited at −1.10 and −1.20 V vs Ag/AgCl produced epitaxial (11$\bar{2}$0) ferrihydrite on epitaxial [110] magnetite on Au(110).

Further work is required to determine the magnetic properties of these electrodeposited magnetite and ferrihydrite films. If the production of ferrimagnetic magnetite, superparamagnetic ferrihydrite, and ferromagnetic iron can be tuned by applying different potentials, then the fabrication of superlattices and layered films for giant magnetoresistance and spintronic devices becomes feasible.

Acknowledgment. The authors acknowledge full support for this research from DOE Grant DE-FG02-08ER46518.